European Conference on Optical Communication (ECOC) 2022 © Optica Publishing Group 2022

Is There an Ideal Plasmonic Modulator Configuration?

Tobias Blatter(1), Yannik Horst(1), Wolfgang Heni(2), Christos Pappas(3), ApostolosTsakyridis(3), George Giamougiannis(3), Marco Eppenberger(1), Manuel Kohli(1), Ueli Koch(1), Miltiadis Moralis-Pegios(3), Nikos Pleros(3) and Juerg Leuthold(1)

(1) ETH Zurich, Institute of Electromagnetic Fields, 8092 Zurich, Switzerland,
(2) Polariton Technologies AG, 8803 Rüschlikon, Switzerland
(3) Department of Informatics, Aristotle University of Thessaloniki, 54124, Thessaloniki, Greece
(Tobias.Blatter@ief.ee.ethz.ch, Juerg.Leuthold@ief.ee.ethz.ch)

Abstract *Resonant and non-resonant modulator configurations are compared for operation with the lowest drive voltage. The ring-assisted Mach-Zehnder modulator is shown to offer a steep slope in the transfer function while delivering an open eye diagram. This enables 220GBd 2PAM plasmonic modulation with record low 0.5V$_p$. ©2022 The Author(s)*

Introduction

Optical modulators are the workhorses of the communications industry. The increasing demand for high-speed optical data transmission and high-throughput optical artificial neurons [1, 2] seeks electro-optical (EO) modulators with transfer functions that feature a steep slope and thereby provide a large optical modulation for smallest voltage swings. Another desirable feature would be a modulator transfer function thatflattens out at the on- and the off-levels to reduce electrical noise.

A large variety of modulator concepts is known to the community. Most often, they fall into the Mach-Zehnder modulator (MZM) or ring modulator (RM) type category [3-5]. Combinations of the two have also been discussed [6-8]. And indeed, the advantages of the various modulator types are well known for Pockels-effect or silicon-based modulators. In the past few years, plasmonic modulators have emerged. They provide bandwidths up to $500\ \mathrm{GHz}$, a footprint below $100\ \mu\mathrm{m}^2$, and power consumption in the atto-joule per bit regime [9-11]. Unfortunately, plasmonic modulators also come with losses. The longer the phase-shift section the larger the losses. The question then is, which configuration offers the largest modulation amplitude for the least voltage swing.[12-15].

In this work, we demonstrate that the ring-assisted MZM (RaMZM) configuration offers the advantages of the MZM with the push-pull operation and flat frequency response in the on- and off-levels while also benefiting from resonant enhancements due the built-in ring. Larger modulation for less power may be achieved. Ultimately, we demonstrate 220 Gbit/s NRZ modulation with record low $V_\mathrm{p} = 0.5\ \mathrm{V}$.

Theory and Device Comparison

Three basic modulator configurations are considered in this study and depicted in Fig. 1. Among which are the racetrack modulator (RM), the conventional MZM and the RaMZM. The RM is known to feature lowest driving voltages due to the resonant enhancement [3]. However, its bandwidth might be limited if ring lengths are overly long, which can be reduced due to the small footprints POH allows.The MZM provides an almost ideal transfer function for on-off keying with a flat plateau at the on- and off-levels and almost zero chirp and enables push-pull operation to save half of the driving voltage. The RaMZM combines the resonant enhancement of the RM with the advantages of the MZM.

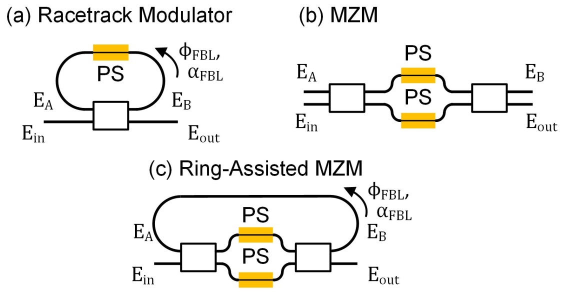

Fig. 1: (a) Racetrack modulator (RM) where the phase is modulated in the ring (feedback loop). (b) Mach-Zehnder modulator (MZM). (c) Ring-assisted Mach-Zehnder modulator (RaMZM) where modulation is enhanced by feedback of light.

The steady-state transfer function (TF) of the three modulator types are plotted in Fig. 2(a)-(b). Mathematically the transfer functions of an input field $E_\mathrm{in}(t)$ to an output field $E_\mathrm{out}(t)$ can be described by

$$\begin{bmatrix} E_\mathrm{out}(t) \\ E_B(t) \end{bmatrix} = \begin{bmatrix} \sigma(t) & \kappa(t) \\ -\kappa^*(t) & \sigma^*(t) \end{bmatrix} \begin{bmatrix} E_\mathrm{in}(t) \\ E_A(t) \end{bmatrix} \quad (1)$$

$$E_A(t) = \alpha_\mathrm{FBL} e^{i\phi_\mathrm{FBL}(t)} E_B(t-\tau), \quad (2)$$

where τ is the round trip time, and α_FBL and ϕ_FBL are the amplitude loss parameter and the accumulated phase within the feedback loop (FBL), respectively [16]. Inserting eq. (2) in

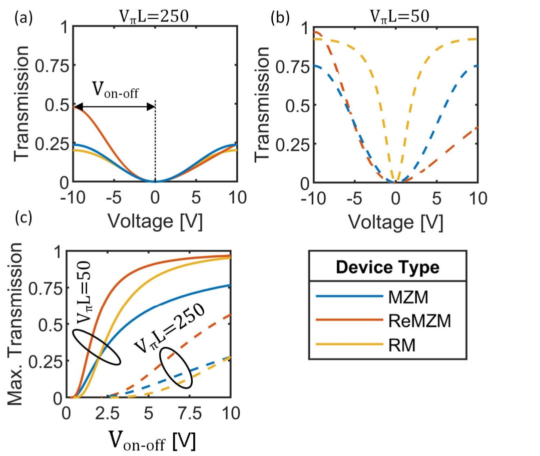

Fig. 3 Transmission plots of plasmonic MZM, the ring-assisted MZM (RaMZM) and the racetrack modulator (RM). (a) Transfer function for modulators with a typical EO-nonlinearity of $V_\pi L^{(\mathrm{PS})} = 250\ \mathrm{V\mu m}$ and (b) a large EO-nonlinearity $V_\pi L^{(\mathrm{PS})} = 50\ \mathrm{V\mu m}$ for a on-off voltage of $V_{\text{on-off}} = 10\ \mathrm{V}$. (c) Maximum transmission achieveable if available $V_{\text{on-off}}$ is increased (i.e. phase-sections can be smaller).

eq. (1) and solving for $T = E_{\mathrm{out}}/E_{\mathrm{in}}$ in steady-state leads to the complex-valued transfer function

$$T = \frac{\sigma(t) - (|\kappa(t)|^2 + |\sigma(t)|^2)\, \alpha_{\mathrm{FBL}} e^{i\phi_{\mathrm{FBL}}(t)}}{1 - \alpha_{\mathrm{FBL}} e^{i\phi_{\mathrm{FBL}}(t)} \sigma^*(t)}. \quad (3)$$

For the RaMZM, ϕ_{FBL} is not modulated. Yet, the coupling coefficients are modulated by

$$\sigma(t) = i\alpha_{\mathrm{MZM}} \sin\left(\frac{V(t)}{V_\pi}\pi + \frac{\varphi_{\mathrm{Bias}}}{2}\right) \quad (4)$$

$$\kappa(t) = i\alpha_{\mathrm{MZM}} \cos\left(\frac{V(t)}{V_\pi}\pi + \frac{\varphi_{\mathrm{Bias}}}{2}\right), \quad (5)$$

where V_π is the voltage required to induce a phase shift of π in a standalone phase shifter (PS), and φ_{Bias} is an offset phase shift in the arms [4, 6]. The coupling losses α_{MZM} is given by the plasmonic loss, which is given by $\alpha_{\mathrm{MZM}} = e^{-\gamma L_{\mathrm{Mod}}}$, where L_{Mod} and γ are the length of the modulator and the plasmonic propagation loss, respectively. Losses in the FBL are low. We set $\alpha_{\mathrm{FBL}} = \alpha_{\mathrm{Phot}}$. The MZM transfer function is also described by eq. (3) by setting $\alpha_{\mathrm{FBL}} = 0$.

For the RM, the coupling coefficients σ and κ in eq. (3) are not modulated. It holds that $|\sigma|^2 + |\kappa|^2 = 1$ for the lossless case. A special case is the so-called critical coupling case where $\sigma_{crit} = \alpha_{\mathrm{FBL}}$. In the critical coupling case a ring modulator can be completely turned off. Modulation is obtained by driving the phase modulator in the ring, i.e. $\phi_{\mathrm{FBL}}(t) = \frac{V(t)}{V_\pi}\pi + \varphi_{\mathrm{Bias}}$. The losses in the FBL are composed of the photonic losses and the plasmonic losses, i.e. $\alpha_{\mathrm{FBL}} = \alpha_{\mathrm{Phot}}\alpha_{\mathrm{MZM}}$.

To compare the concepts, we kept the voltage-length product of the phase shifter ($V_\pi L^{(\mathrm{PS})}$), the ring length ($80\ \mathrm{\mu m}$), the photonic ($4\ \mathrm{dBcm^{-1}}$) and plasmonic ($\gamma \cong 0.5\ \mathrm{dB\mu m^{-1}}$) propagation losses constant.

First, we consider the case where all

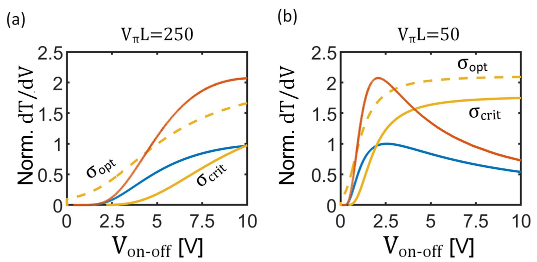

Fig. 2 Performance study of the MZM, the RaMZM and the critical (solid line) and non-critical (dashed line) coupled RM. (a) The transfer functions' steepest slope for modulators optimized for low and large on-off voltage of $V_{\text{on-off}}$, assuming typical EO-nonlinearity and (b) assuming strong EO-nonlinearity.

modulator configurations are designed to operate with the same 10 V swing from on to off. This could e.g., be obtained by modulating a signal by $\pm V_{\text{On-Off}}/2 = \pm 5\ \mathrm{V}$ around an offset bias of -5 V, see Fig. 3(a) and (b). The plot in Fig. 2(a) shows the transfer function for a typical $V_\pi L^{(\mathrm{PS})} = 250\ \mathrm{V\mu m}$. It can be seen that the RaMZM offers the highest transmission output. It is around twice as large as the MZM's and RM output power. Also, it offers the steepest slope and therefore the largest modulation for the least voltage swing. However, if we anticipate a trend towards higher electro-optical (EO) non-linear coefficients with $V_\pi L^{(\mathrm{PS})} = 50\ \mathrm{V\mu m}$, the required PS length can be reduced. The reduction in modulator length results in a more pronounced resonance. Thereby the ring enhanced modulator concepts the RaMZM and RM offer the highest max. transmission, see Fig. 2(c). The RM now offers the steepest slope, while the RaMZM offers a steep slope while still offering the flat response at the on- and off-levels.

In a second analysis, we elaborate on the modulation behaviour. For that, we operate each configuration in the working point (WP) with the highest slope (dT/dV) in their TF. In Fig. 3(a) and Fig. 3(b) the highest slope for typical ($V_\pi L^{(\mathrm{PS})} = 250\ \mathrm{V\mu m}$) and strong EO-nonlinearity ($V_\pi L^{(\mathrm{PS})} = 50\ \mathrm{V\mu m}$) is shown, respectively. The graphs are plotted for a given on-off voltage. I.e. if low on-off voltages are required, then the modulators have to be long (which comes at the price of higher losses). Conversely, if sufficient voltage levels are available, then the phase-modulation section can be short. It must be noted that the devices do not need to be driven with the full on-off-voltage swing, as the steepness indicates the achievable optical modulation amplitude (OMA) for small driving voltages. In both cases, the RaMZM features the highest slope among the considered types. In particular, the RaMZM has an increase in the slope by a factor of two compared to the MZM.

However, if we allow non-critical coupling of the RM, and hence sacrifice the possibility to achieve perfect extinction, the RM offers similar

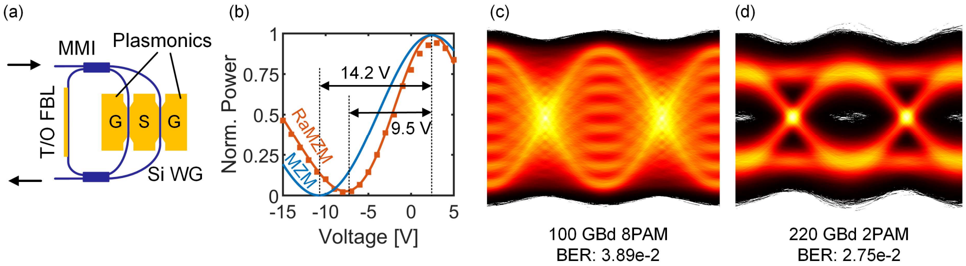

Fig. 4: (a) Sketch of the fabricated RaMZM device, with a thermo-optical (T/O) heater controlling the FBL's phase. (b) Measured intensity for different voltages (dots) and fit of the transfer function (red line). The blue curve shows the transfer function of the non-resonant MZM, showing a 33% decrease of the required oo-voltage. (c-d) Transmitted eye diagrams after DSP of the measured 100 GBd 8PAM and 220 GBd 2PAM NRZ signal showing BER below the SD-FEC limit.

steepnesses compared to the RaMZM. Particularly, such steep slopes are obtained if on-off voltages are high and the phase-shift section is small (i.e. the more resonant the ring.)

Ring-Assisted Mach-Zehnder (RaMZM) Exp.

We fabricated and measured an implementation of the RaMZM in a silicon-on-insulator platform and exploited the Pockel's effect of an organic EO material in plasmonic PS as sketched in Fig.4(a) [17]. The coupling section consists of two 2x2 MMIs, splitting the light into two imbalanced arms, allowing to set the working point by choice of the wavelength. The plasmonic PS operates in a push-pull configuration, and a thermo-optical phase shifter allows to adjust the phase in the FBL. The on-chip device loss was measured to be $8.5\ \mathrm{dB}$ and the photonic losses in the $116\ \mu\mathrm{m}$ long FBL was estimated to be $\alpha_{\mathrm{Phot}} = 0.9946$. The plasmonic propagation losses in the $10\ \mu\mathrm{m}$ long modulator were $0.52\ \mathrm{dB}\mu\mathrm{m}^{-1}$ for a slot width of $105\ \mathrm{nm}$. Fitting the transfer function to the measurement reveals a V_π of $28\ \mathrm{V_{pp}}$ as shown in Fig. 4(b), corresponding to $V_\pi L^{(\mathrm{PS})} = 286\ \mathrm{V}\mu\mathrm{m}$. The on-off-voltage was measured to be $9.5\ \mathrm{V_{pp}}$. In contrast, an MZM with the same EO and plasmonic properties, would require an on-off-voltage of $14.2\ \mathrm{V_{pp}}$. The RaMZM therefore offers a driving-voltage-advantage of $33\,\%$ over the MZM. Note that the plasmonic modulator is designed as a high-impedance load, utilizing twice the applied 50 Ω drive voltage. A 50 Ω-matched driver needs to provide 4.75 $\mathrm{V_{pp}}$ in order to switch the RaMZM from the on- to the off-state.

High-Speed Operation of RaMZM

To verify the advantage of the RaMZM over the MZM we perform high-speed modulation experiments with with low voltage (without additional driver amplifier) signals. For the test, we deployed a C-band laser, a $256\ \mathrm{GSas}^{-1}$, $70\ \mathrm{GHz}$ arbitrary waveform generator (AWG) to drive the modulator with a $220\ \mathrm{Gbd}$ 2PAM signal and a $100\ \mathrm{Gbd}$ 8PAM signal and a direct detection receiver. The receiver is composed of an erbium-doped fiber amplifier, a bandpass filter, a $145\ \mathrm{GHz}$ photodiode and a $256\ \mathrm{GSas}^{-1}$, 113 GHz digital sampling oscilloscope. The driving voltage had a low peak voltage of $0.5\ \mathrm{V_p}$ (measured into $50\ \Omega$) and the laser power was $12\ \mathrm{dBm}$. For 2PAM modulation, the offline digital signal processing (DSP) included a static finite impulse reponse filter to correct the frequency response of the AWG, followed by a timing recovery, a linear T/2-spaced feed-forward equalizer (FFE) with 151 filter taps, a non-linear maximum-a-posteriori equalizer and a second linear T-spaced FFE with 251 taps. For the 8PAM signal, the DSP consists of a timing recovery, a third-order volterra equalizer with 151, 51 and 15 taps, and a T-spaced FFE with 351 taps.

We report $100\ \mathrm{GBd}$ 8PAM NRZ data modulation with a BER of $3.89 \cdot 10^{-3}$, and $220\ \mathrm{GBd}$ 2PAM NRZ with a BER of $2.75 \cdot 10^{-2}$. For both experiments, the BER was below the soft-decision forward-error-correction (SD-FEC) limit of $4 \cdot 10^{-2}$, see Fig.4(c)-(d). We show for the first time single-drive modulation without an additional driving amplifier at $220\ \mathrm{GBd}$ 2PAM NRZ with POH technology .[12, 18].

Conclusions

We showed a ring-assisted MZM. The modulator offers on-off modulation with a 33 % voltage swing reduction if compared to a non-resonant MZM. The RaMZM enables driverless IM/DD data transmission up to $100\ \mathrm{GBd}$ 8PAM and $220\ \mathrm{GBd}$ 2PAM NRZ below the SD-FEC limit, with driving voltages as low as $V_\mathrm{p} = 0.5\ \mathrm{V}$.

Acknowledgements

ETH Zurich acknowledges funding by the grants H2020 Project 871391 PlasmoniAC and H2020 Project 863155 NEBULA and thanks Polariton Technologies for fabricating the devices. The devices were designed using Polariton's PDK. Polariton thanks NLM Photonics for the supply of the organic EO material. For laboratory automation the FOSS LabExT was used. We thank the Binning and Rohrer Nanotechnology Center (BRNC).

References

[1] A. R. Totović, G. Dabos, N. Passalis, A. Tefas, and N. Pleros, "Femtojoule per MAC Neuromorphic Photonics: An Energy and Technology Roadmap," *IEEE Journal of Selected Topics in Quantum Electronics,* vol. 26, no. 5, pp. 1-15, 2020, doi: 10.1109/JSTQE.2020.2975579.

[2] C. Minkenberg, R. Krishnaswamy, A. Zilkie, and D. Nelson, "Co-packaged datacenter optics: Opportunities and challenges," *IET Optoelectronics,* vol. 15, no. 2, pp. 77-91, 2021, doi: https://doi.org/10.1049/ote2.12020.

[3] J. Müller *et al.*, "Optical peaking enhancement in high-speed ring modulators," (in eng), *Sci Rep,* vol. 4, p. 6310, Sep 11 2014, doi: 10.1038/srep06310.

[4] W. D. Sacher and J. K. S. Poon, "Dynamics of microring resonator modulators," *Opt. Express,* vol. 16, no. 20, pp. 15741-15753, 2008/09/29 2008, doi: 10.1364/OE.16.015741.

[5] J. Witzens, "High-Speed Silicon Photonics Modulators," *Proceedings of the IEEE,* vol. 106, no. 12, pp. 2158-2182, 2018, doi: 10.1109/JPROC.2018.2877636.

[6] A. Yariv, "Critical coupling and its control in optical waveguide-ring resonator systems," *IEEE Photonics Technology Letters,* vol. 14, no. 4, pp. 483-485, 2002, doi: 10.1109/68.992585.

[7] W. D. Sacher *et al.*, "Coupling modulation of microrings at rates beyond the linewidth limit," *Opt. Express,* vol. 21, no. 8, pp. 9722-9733, 2013/04/22 2013, doi: 10.1364/OE.21.009722.

[8] R. Yang, L. Zhou, H. Zhu, and J. Chen, "Low-voltage high-speed coupling modulation in silicon racetrack ring resonators," *Opt. Express,* vol. 23, no. 22, pp. 28993-29003, 2015/11/02 2015, doi: 10.1364/OE.23.028993.

[9] W. Heni *et al.*, "Plasmonic IQ modulators with attojoule per bit electrical energy consumption," *Nature Communications,* vol. 10, no. 1, p. 1694, 2019/04/12 2019, doi: 10.1038/s41467-019-09724-7.

[10] M. Burla *et al.*, "500 GHz plasmonic Mach-Zehnder modulator enabling sub-THz microwave photonics," vol. 4, no. 5, p. 056106, 2019, doi: 10.1063/1.5086868.

[11] C. Haffner *et al.*, "Plasmonic organic hybrid modulators—scaling highest speed photonics to the microscale," vol. 104, no. 12, pp. 2362-2379, 2016.

[12] M. Eppenberger *et al.*, "Plasmonic Racetrack Modulator Transmitting 220 Gbit/s OOK and 408 Gbit/s 8PAM," in *2021 European Conference on Optical Communication (ECOC)*, 13-16 Sept. 2021 2021, pp. 1-4, doi: 10.1109/ECOC52684.2021.9605911.

[13] A. Messner *et al.*, "High-Speed Plasmonic Modulator for Simultaneous C- and O-Band Modulation with Simplified Fabrication," in *Optical Fiber Communication Conference (OFC) 2020*, San Diego, California, 2020/03/08 2020: Optical Society of America, in OSA Technical Digest, p. M1D.3, doi: 10.1364/OFC.2020.M1D.3. [Online]. Available: http://www.osapublishing.org/abstract.cfm?URI=OFC-2020-M1D.3

[14] G. Li *et al.*, "Ring Resonator Modulators in Silicon for Interchip Photonic Links," *IEEE Journal of Selected Topics in Quantum Electronics,* vol. 19, no. 6, pp. 95-113, 2013, doi: 10.1109/JSTQE.2013.2278885.

[15] A. Messner *et al.*, "100 Gbit/s NRZ Data Modulation in Plasmonic Racetrack Modulators on the Silicon Photonic Platform," in *2020 European Conference on Optical Communications (ECOC)*, 6-10 Dec. 2020 2020, pp. 1-3, doi: 10.1109/ECOC48923.2020.9333272.

[16] A. Yariv, "Universal relations for coupling of optical power between microresonators and dielectric waveguides," *Electronics Letters,* vol. 36, pp. 321-322, 03/17 2000, doi: 10.1049/el:20000340.

[17] H. Xu *et al.*, "Ultrahigh Electro-Optic Coefficients, High Index of Refraction, and Long-Term Stability from Diels–Alder Cross-Linkable Binary Molecular Glasses," *Chemistry of Materials,* vol. 32, no. 4, pp. 1408-1421, 2020/02/25 2020, doi: 10.1021/acs.chemmater.9b03725.

[18] W. Heni *et al.*, "Ultra-High-Speed 2:1 Digital Selector and Plasmonic Modulator IM/DD Transmitter Operating at 222 GBaud for Intra-Datacenter Applications," *J. Lightwave Technol.,* vol. 38, no. 9, pp. 2734-2739, 2020, doi: 10.1109/JLT.2020.2972637.